Angewandte Chemie
Eine Zeitschrift der Gesellschaft Deutscher Chemiker

Supporting Information

Amorphous Aluminosilicate Nanosheets as Universal Precursors for the Synthesis of Diverse Zeolite Nanosheets for Polymer-Cracking Reactions

K. Sasaki, J. A. H. Gaitan, T. Okue, S. Matoba, Y. Tokuda, K. Miyake, Y. Uchida, N. Nishiyama*

Supporting Information

69451 Weinheim, Germany

Amorphous Aluminosilicate Nanosheets as Universal Precursors for the Synthesis of Diverse Zeolite Nanosheets for Polymer-Cracking Reactions

Koki Sasaki, Jose Andres Hernandez Gaitan, Tsuyoshi Okue, Shotaro Matoba, Yuki Tokuda, Koji Miyake, Yoshiaki Uchida,* and Norikazu Nishiyama

Abstract: Zeolites catalyze some reactions in their molecular-sized pores, but large molecules can react only on their external surface. Zeolite-nanosheets (NSs) have been developed as catalysts for large molecules. The previously reported methods to synthesize zeolite-NSs are specialized for each crystal. Here we propose a new method to synthesize various zeolite-NSs from the same amorphous aluminosilicate NSs (AAS-NSs) as a universal precursor. We successfully synthesized the unprecedented AAS-NSs in the hydrophilic space of the stable hyperswollen lyotropic lamellar (HL) phase. The four zeolite types could be obtained from the single-species AAS-NSs. These results imply that this method enables us to synthesize almost all types of zeolite-NSs. Moreover, the synthesized CHA-NSs have great potential for various applications because of their thickness and large external surface area.

SUPPORTING INFORMATION

Table of Contents

Experimental Procedures

Materials

Decane, 1-pentanol, ethanol, *p*-octylbenzenesulfonate (SOBS), tetraethyl orthosilicate (TEOS), sodium hydroxide (NaOH) and aluminum isopropoxide (Al(O-*i*-Pr)$_3$) were purchased from Wako Pure Chemical Industries Co. 20 – 25 wt% tetrapropylammonium hydroxide (TPAOH) was purchased from Tokyo Chemical Industry Co., Ltd. Low density polyethylene powder (LDPE) (500 μm) was purchased from Alfa Aesar. 25 wt% N,N,N-trimethyl-1-adamantanammonium hydroxide (TMAdaOH) was donated from SACHEM, Inc. The water used was obtained from a water purifier (Direct-Q UV) with a resistivity of 18.2 MΩcm.

Synthesis methods

Amorphous aluminosilicate nanosheets synthesis

Amorphous aluminosilicate nanosheets (AAS-NSs) were synthesized in the hyperswollen lyotropic lamellar (HL) phases of the decane solutions of SOBS (0.95 wt %), 1-pentanol (8.4 wt %), and deionized water (1.1 wt %). NaOH (9.4×10^{-3} wt%), TEOS (0.25 wt%), and Al(O-*i*-Pr)$_3$ (1.2×10^{-2} wt%) was added to the decane solution and stirred at 60ºC for 24 hours. After stirred, we added ethanol to this solution and did centrifugal separation. After drying at 90ºC for 24 h, the white powder, mixture of AAS-NSs and SOBS, was collected.

CHA type zeolite nanosheets synthesis

TMAdaOH solution (1.4 g) was added to the AAS-NSs coated with SOBS (0.215 g) and mixed. After drying at 90ºC for 24 h, the resulting gel was put in a Teflon-lined stainless steel autoclave with water separately where the reaction take place with the steam produced. Treatment was carried out at 160ºC for 96 h. After the autoclave was cooled down at room temperature, the product was washed with deionized water and dried 90ºC. The catalyst was calcined in air at 550ºC for 5 h to eliminate the organic template.

PHI type zeolite nanosheets synthesis

TMAdaOH solution (1.4 g) was added to the AAS-NSs coated with SOBS (0.215 g) and mixed. After drying at 90ºC for 24 h, the resulting gel was put in a Teflon-lined stainless steel autoclave with water separately where the reaction take place with the steam produced. Treatment was carried out at 160ºC for 48 h. After the autoclave was cooled down at room temperature, the product was washed with deionized water and dried 90ºC. The catalyst was calcined in air at 550ºC for 5 h to eliminate the organic template.

SOD type zeolite nanosheets synthesis

NaOH (0.015 g) and water (0.2 g) were added to the AAS-NSs coated with SOBS (0.215 g) and put in a Teflon-lined stainless steel autoclave with water separately where the reaction take place with the steam produced. Treatment was carried out at 180ºC for 48 h. After the autoclave was cooled down at room temperature, the product was washed with deionized water and dried 90ºC.

MFI type zeolite nanosheets synthesis

TPAOH solution (1.2 g) was added to the mixture of AAS-NSs coated with SOBS (0.215 g) and mixed. After drying at 90ºC for 24 h, the resulting gel was put in a Teflon-lined stainless steel autoclave with water separately where the reaction take place with the steam produced. Treatment was carried out at 180ºC for 48 h. After the autoclave was cooled down at room temperature, the product was washed with deionized water and dried 90ºC. The product was calcined in air at 550ºC for 5 h to eliminate the organic template.

Catalytic test

LDPE was dissolved in the toluene at 70ºC, and added the toluene dispersion of CHA-NSs. After drying the solution, we obtained the mixture of LDPE and CHA-NSs. The LDPE cracking test was carried out using a fixed-bed reactor made of quartz glass (id 4 mm) with a continuous-flow system under atmospheric pressure at 500ºC. Helium gas was introduced at 10 mL min^{-1}. The products were analyzed online with a Shimadzu GC-2025 gas chromatograph equipped with a flame ionization detector.

Characterization methods

X-ray Diffraction (XRD) Measurements

The crystal structures were estimated from XRD patterns collected using a PANalytical X'Pert PRO diffractometer with Cu Kα radiation, operated at 45 kV and 40 mA. The scan range was from 30º to 45º (2θ) at $0.10^{o}s^{-1}$. The full width at half maximum was calculated using X'Pert Data Viewer.

Dynamic Light Scattering (DLS)

The distributions of samples were measured by DLS using ELSZ-2000 (Otsuka Electronics Co., Ltd.) at 25°C.

Atomic Force Microscopy (AFM)

AFM images were obtained using a Veeco Instruments MMAFM-2. The samples were deposited on freshly exfoliated mica sheets as substrates. We measured 15 samples and calculated the average and standard deviation of the size and thickness, respectively.

SUPPORTING INFORMATION

Transmission Electron Microscopy (TEM)
TEM images were obtained using a Hitachi H-800 at 200 kV.

Field Emission Transmission Electron Microscopy (FE-TEM)
FE-TEM images were obtained using a Hitachi HF-2000 at 200 kV.

Scanning Electron Microscopy and Energy Dispersive X-ray Spectroscopy (SEM-EDX)
SEM-EDX images were obtained using a JEOL JCM-7000 microscope at 15 kV.

Nitrogen adsorption isotherms
The porosity of the products was characterized by nitrogen adsorption measurements using a BELSORPmax (MicrotracBEL).

Ammonia's Temperature-Programmed Deposition (NH_3-TPD)
The acidic properties of the samples were analyzed by NH_3-TPD measurement using a MicrotracBEL BELCAT II as follows. About 0.05 g of sample was pretreated under a He flow at 773 K for 1 h and then cooled to the adsorption temperature of 373 K. A gas mixture of NH_3 and He (1 vol% of NH_3) was introduced into the sample cell for 1 h. Subsequently, He (30 cm^3 (STP) min^{-1}) was passed through the sample to remove weakly adsorbed NH_3 for 1 h. Then, the sample was heated up to 973 K at a rate of 10 K min^{-1}. The desorbed NH_3 signal was recorded on a quadrupole mass spectrometer (MicrotracBEL, BELMass).

SUPPORTING INFORMATION

Results and Discussion

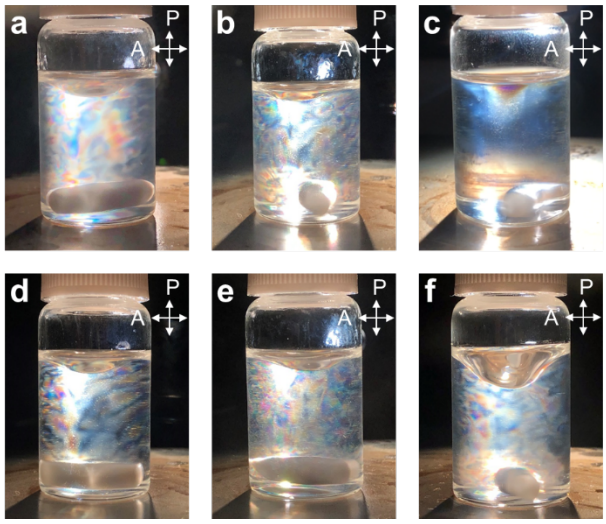

Figure S1. Liquid crystalline textures of hyperswollen lyotropic lamellar phases. These are decane solutions of SOBS (0.95 wt%), 1-pentanol (8.4 wt%), and water (1.1 wt%) with the following additives at 60°C: a) No additives, b) NaOH (9.4×10^{-3} wt%), c) NaOH (3.8×10^{-2} wt%), d) NaOH (9.4×10^{-3} wt%) and TEOS (0.25 wt%), e) NaOH (9.4×10^{-3} wt%) and Al(O-*i*-Pr)$_3$ (1.2×10^{-2} wt%), and f) NaOH (9.4×10^{-3} wt%), TEOS (0.25 wt%) and Al(O-*i*-Pr)$_3$ (1.2×10^{-2} wt%). Samples are placed between crossed polarizers.

Table S1. Specific surface area (S_{total}), external surface area (S_{ext}) and pore volume (V_{total}) of AAS bulk samples and AAS-NSs after filtration measured by nitrogen adsorption isotherms.

	S_{total}[a] / m^2g^{-1}	S_{ext}[b] / m^2g^{-1}	V_{total}[b] / cm^3g^{-1}
AAS bulk samples	35	1.3	0.07
AAS-NSs	63	63	0.75

[a] BET surface area calculated using the BET method applied to the nitrogen adsorption isotherm.

[b] S_{ext}, and V_{total} calculated using the α_s-plot method applied to the nitrogen adsorption isotherm.

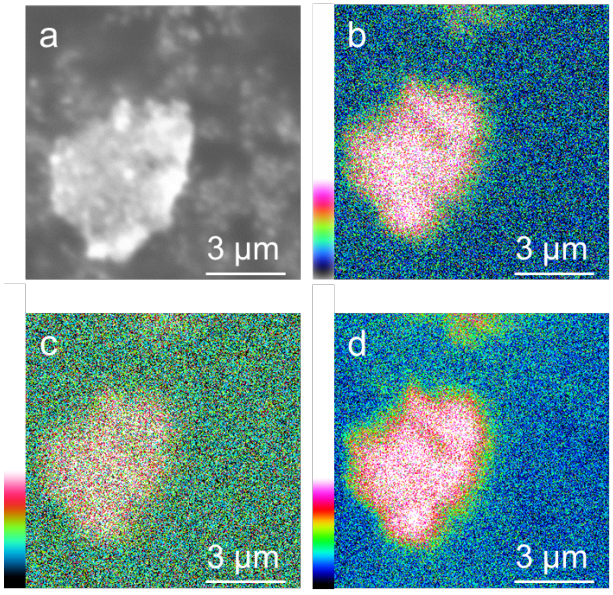

Figure S2. SEM-EDX photographs of one of the synthesized AAS-NSs. a) SEM photograph of one of the synthesized AAS-NSs. EDX mapping of b) silicon, c) aluminum, and d) oxygen elements in one of the synthesized AAS-NSs.

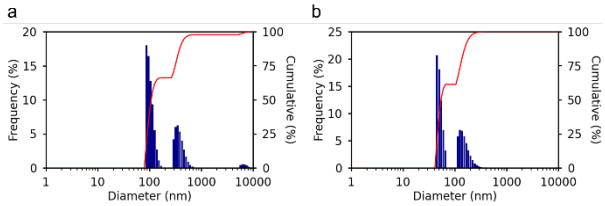

Figure S3. DLS analysis. a) AAS-NSs after centrifugal separation. b) AAS-NSs separated by filtration.

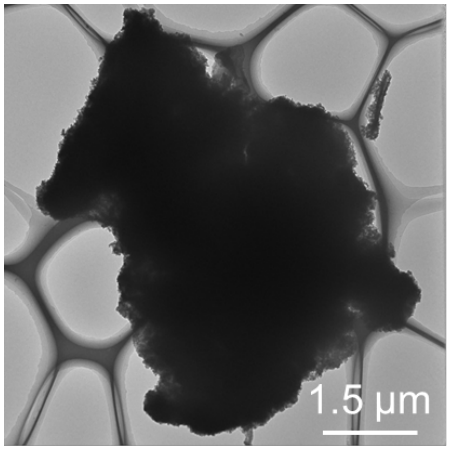

Figure S4. TEM photograph of a particle in the obtained white powder crystalizing after washing SOBS.

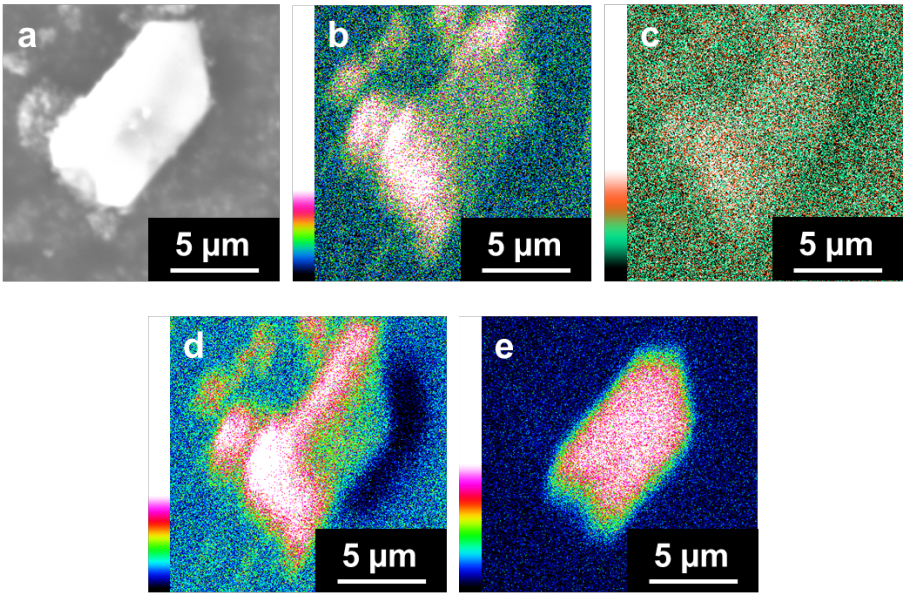

Figure S5. SEM-EDX photographs of one of the synthesized AAS-NSs coated with SOBS. a) SEM photograph of one of the synthesized AAS-NSs. EDX mapping of b) silicon, c) aluminum, d) oxygen, and e) sulfur elements in one of the synthesized AAS-NSs.

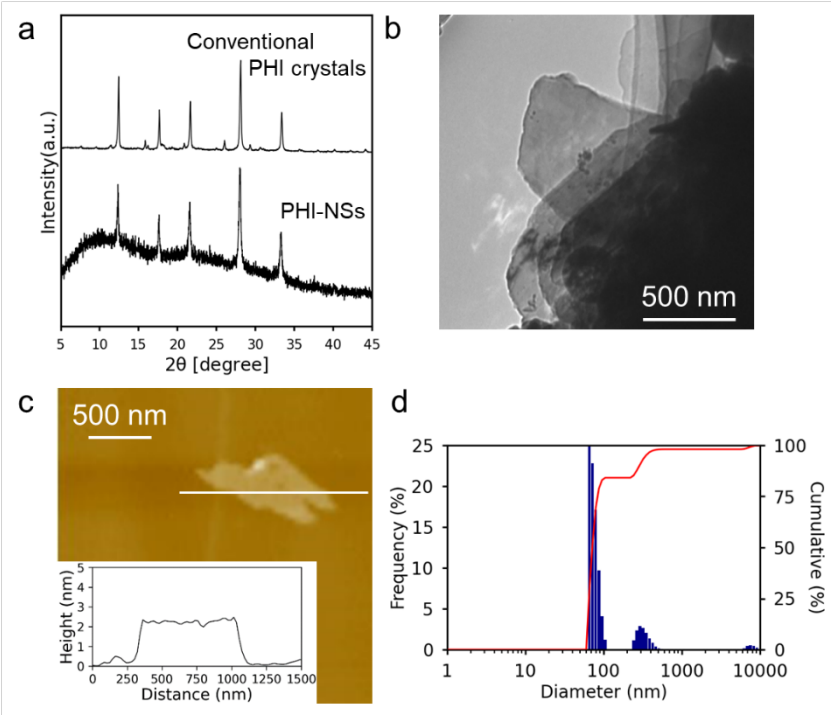

Figure S6. Characterization of synthesized PHI-NSs. a) XRD pattern of PHI-NSs. b) TEM photograph of one of the synthesized PHI-NSs. c) AFM photograph and cross section of one of the synthesized PHI-NSs. d) DLS analysis of PHI-NSs.

Table S2. XRD peak positions and full widths at half maximum for CHA-NSs and conventional CHA crystals.

Peak (2θ)	Full width at half maximum (°)	
	CHA-NSs	Conventional CHA crystals
9.6	0.182	0.128
13.0	0.203	0.147
14.1	0.213	0.158
16.2	0.213	0.158
17.9	0.183	0.183
20.8	0.213	0.174
23.3	0.200	0.169
25.2	0.260	0.206
26.2	0.237	0.207
28.0	0.311	0.195
28.4	0.134	0.179

Table S3. XRD peak positions and full widths at half maximum for PHI-NSs and conventional PHI crystals.

Peak (2θ)	Full width at half maximum (°)	
	PHI-NSs	Conventional PHI crystals
12.4	0.195	0.143
17.7	0.187	0.152
21.6	0.281	0.162
28.1	0.296	0.207
33.3	0.299	0.201

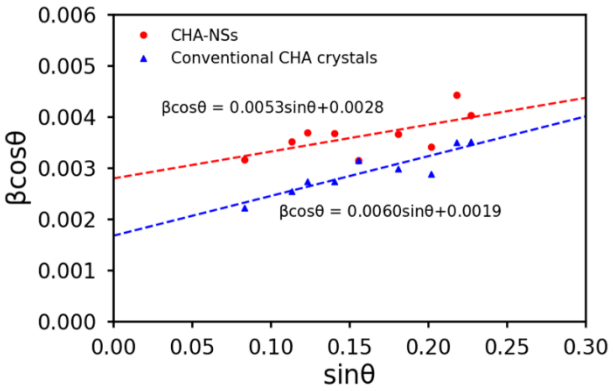

Figure S7. Williamson-Hall plots of CHA-NSs (red) and conventional CHA crystals (blue). In the equations, β is full width at half maximum, η is internal strain, *K* is Scherrer constant, λ is the X-ray wavelength, and *D* is crystallite size. The Scherrer constant used was 0.94. The estimated *D*s for CHA-NSs and conventional CHA crystals are 51 nm and 76 nm, respectively.

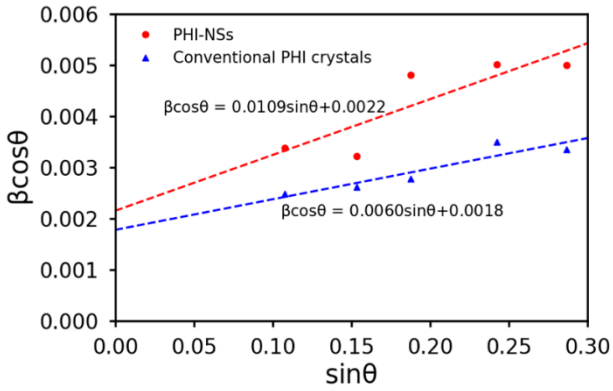

Figure S8. Williamson-Hall plots of PHI-NSs (red) and conventional PHI crystals (blue). In the equations, β is full width at half maximum, η is internal strain, *K* is Scherrer constant, λ is the X-ray wavelength, and *D* is crystallite size. The Scherrer constant used was 0.94. The estimated *D*s for PHI-NSs and conventional PHI crystals are 66 nm and 81 nm, respectively.

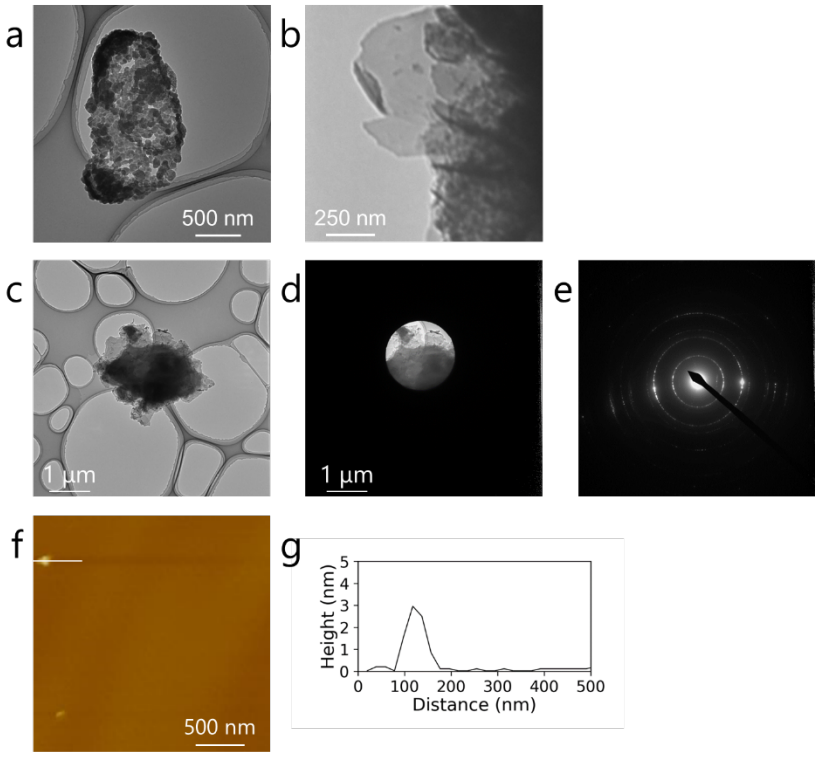

Figure S9. TEM and AFM photographs of PHI-NSs. TEM photographs of a) small PHI-NSs and b) large PHI-NSs. TEM photographs c) without and d) with selected area diffraction aperture. e) SAED pattern. f) AFM photograph and g) cross section of one of the synthesized PHI-NSs.

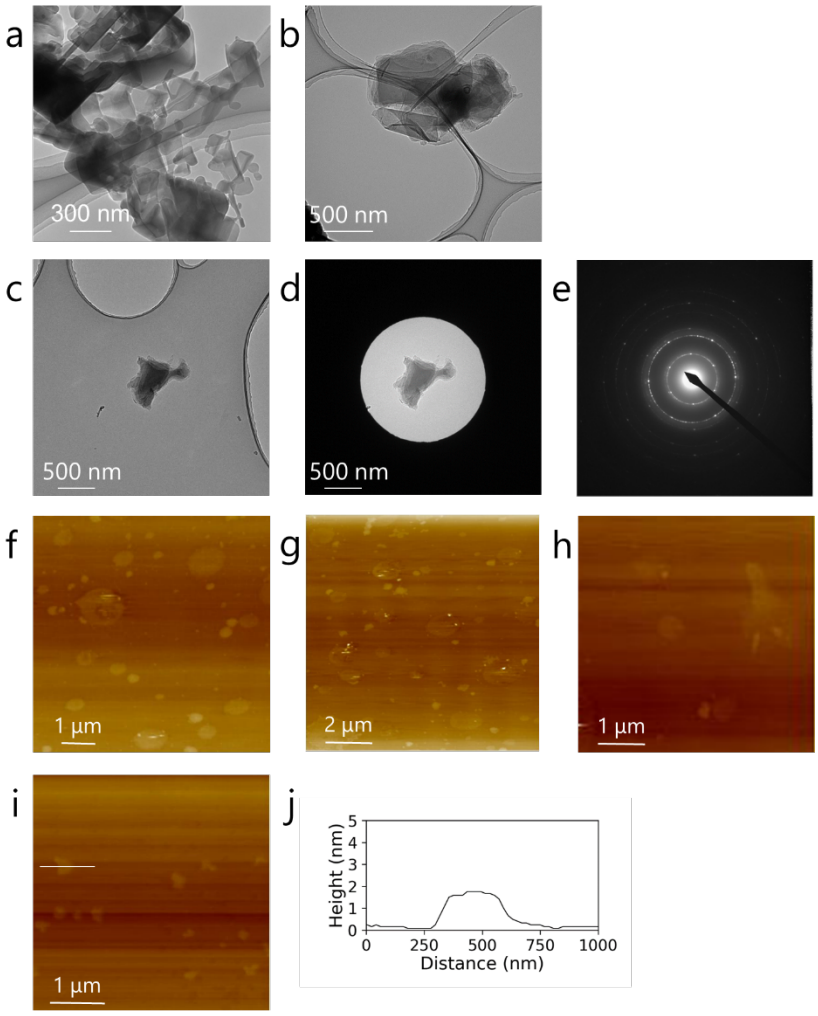

Figure S10. TEM and AFM photographs of CHA-NSs. TEM photographs of a) small CHA-NSs and b) large CHA-NSs. TEM photographs c) without and d) with selected area diffraction aperture. e) SAED pattern. f)-i) AFM photograph and j) cross section of one of the synthesized CHA-NSs.

a

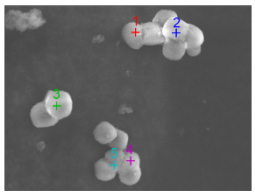

	Al	Si
1	2.26	20.85
2	2.10	17.10
3	2.02	17.29
4	2.78	22.57
5	2.63	22.23
Average	2.36	20.01

Si/Al = 8.5

b

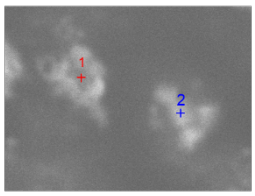

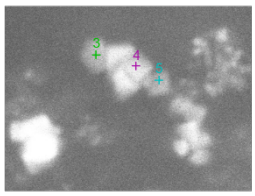

	Al	Si
1	0.41	2.65
2	0.36	2.61
3	0.29	3.23
4	0.29	3.65
5	0.28	3.18
Average	0.33	3.06

Si/Al = 9.3

Figure S11. SEM-EDX spectra and Si/Al ratio for CHA zeolites. a) Conventional CHA crystals. b) CHA-NSs.

a

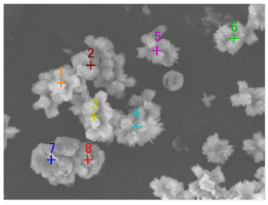

	Na	K	Al	Si
1	3.51	3.67	8.43	17.17
2	3.49	2.82	7.60	15.77
3	3.41	2.66	7.58	15.37
4	3.50	1.86	6.54	13.08
5	3.18	3.00	8.39	18.39
6	3.10	5.95	11.57	24.98
7	3.21	1.81	6.37	12.51
8	2.20	1.68	4.79	9.33
Average	3.20	2.93	7.66	15.82

Si/Al = 2.67

b

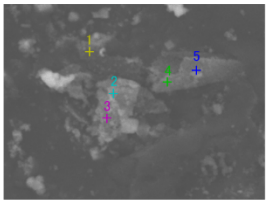

	Na	Al	Si
1	0	1.12	3.81
2	0	0.88	4.00
3	0.12	0.57	0.89
4	0.12	4.38	10.41
5	0.09	4.64	11.14
Average	0.11	1.95	8.09

Si/Al = 2.61

Figure S12. SEM-EDX spectra and Si/Al ratio for PHI zeolites. a) Conventional PHI crystals. b) PHI-NSs.

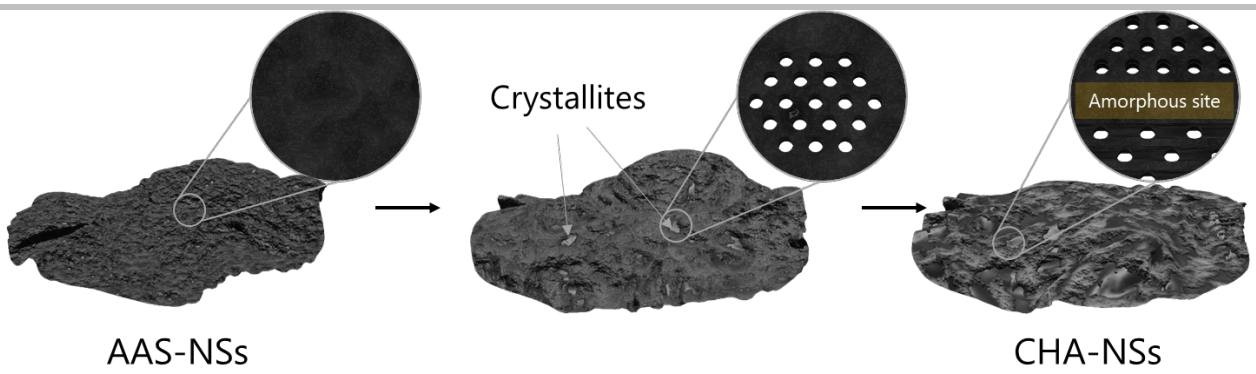

Figure S13. Schematic illustration of the crystallization process of the CHA-NSs. Crystallization begins at many points, and each crystallite grows individually, resulting in the residual amorphous sites at the boundaries between the crystallites due to inconsistency.

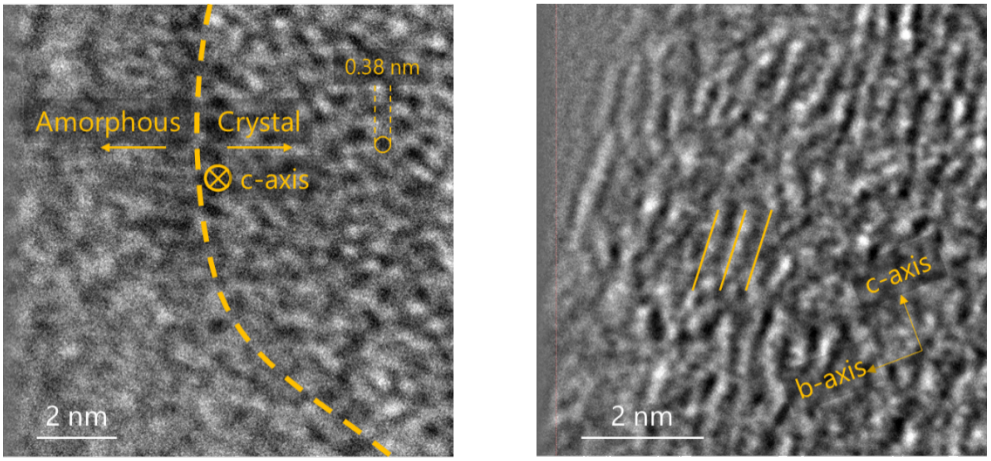

Figure S14. FE-TEM photographs for CHA-NSs.

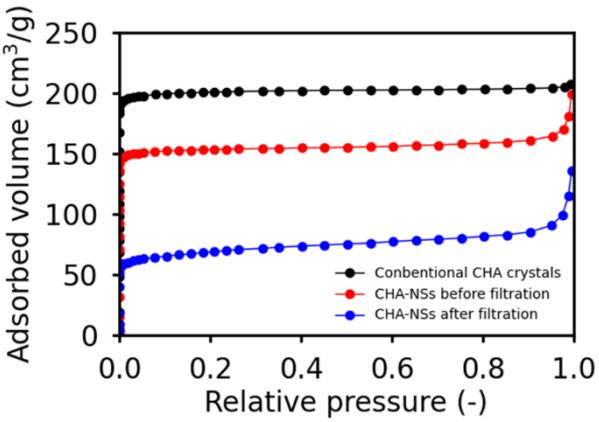

Figure S15. Nitrogen adsorption isotherms of CHA-NSs before (red) and after (blue) filtration and conventional CHA crystals (black).

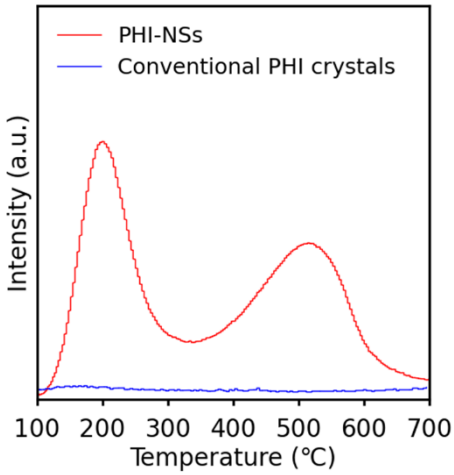

Figure S16. NH_3-TPD profiles of PHI-NSs (red) and conventional PHI crystals (blue).

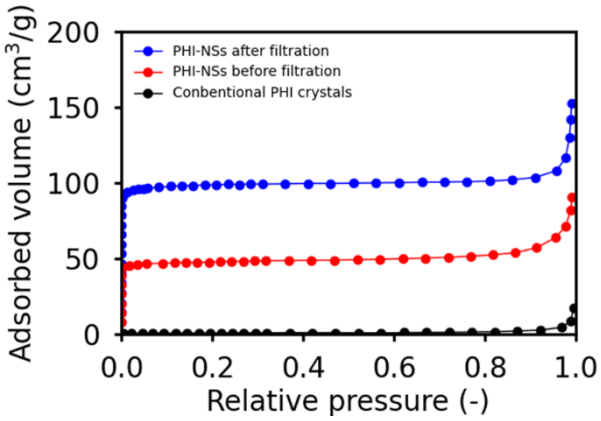

Figure S17. Nitrogen adsorption isotherms for PHI-NSs before (red) and after (blue) filtration and conventional PHI crystals (black).

Table S4. Specific surface area (S_{total}), external surface area (S_{ext}) and pore volume (V_{total}) of conventional PHI crystals, PHI-NSs before filtration, and PHI-NSs after filtration measured by nitrogen adsorption isotherms.

	S_{total}[a] / m^2g^{-1}	S_{ext}[b] / m^2g^{-1}	V_{total}[b] / cm^3g^{-1}
Conventional PHI crystals	3	3	0
PHI-NSs before filtration	153	11	0.07
PHI-NSs after filtration	319	16	0.14

[a] Surface area calculated using BET method (BET surface area) applied to the nitrogen adsorption isotherm.

[b] S_{ext} and V_{total} calculated using the *t*-plot method applied to the nitrogen adsorption isotherm.

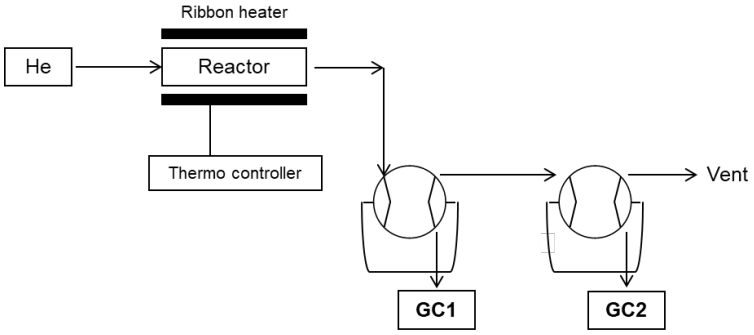

Figure S18. Experimental setup for the LDPE cracking reaction test.

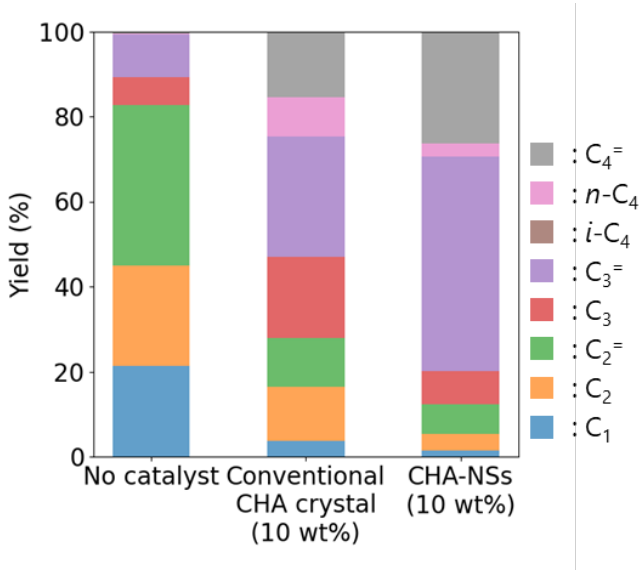

Figure S19. Distribution of the products smaller than pentene in LDPE cracking reactions without catalysts and with conventional CHA crystals (10 wt%) or CHA-NSs (10 wt%).

SUPPORTING INFORMATION

Table S5. Product distribution in LDPE cracking reactions without catalysts and with conventional CHA crystals (10 wt%) or CHA-NSs (10 wt%). Product distribution with (left side) and without (right side) large molecules.

	No catalyst	Conventional CHA crystals (10 wt%)	CHA-NSs (10 wt%)	No catalyst	Conventional CHA crystals (10 wt%)	CHA-NSs (10 wt%)
C_1	21.2	1.69	0.91	21.4	3.71	1.40
C_2	23.4	5.75	2.59	23.6	12.6	3.98
$C_2^=$	37.4	5.23	4.57	37.8	11.5	7.01
C_3	6.42	8.66	5.09	6.48	19.1	7.81
$C_3^=$	10.0	12.9	32.9	10.1	28.3	50.4
i-C_4	0	0	0	0	0	0
n-C_4	0.174	4.19	1.93	0.176	9.22	2.95
$C_4^=$	0.453	7.04	17.2	0.457	15.5	26.4
C_5	0.316	9.34	7.83			
Others	0.601	45.2	27.0			
Sum	100	100	100	100	100	100

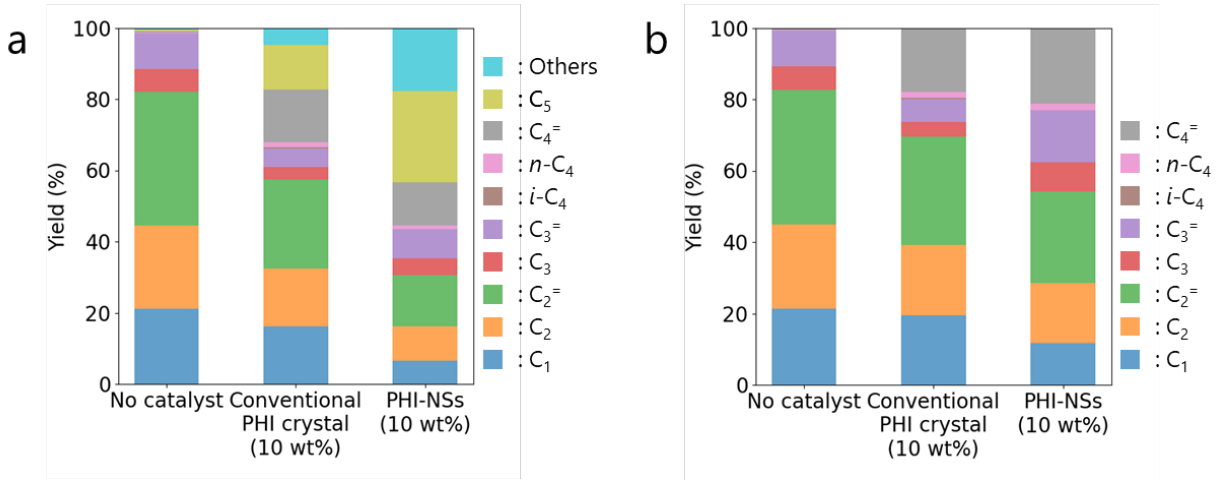

Figure S20. Product distribution in LDPE cracking reactions without and with conventional PHI crystals (10 wt%) or PHI-NSs (10 wt%). Product distribution a) with and b) without large molecules.

SUPPORTING INFORMATION

Table S6. Product distribution in LDPE cracking reactions without catalysts and with conventional PHI crystals (10 wt%) or PHI-NSs (10 wt%). Product distribution with (left side) and without (right side) large molecules.

	No catalyst	Conventional PHI crystals (10 wt%)	PHI-NSs (10 wt%)	No catalyst	Conventional PHI crystals (10 wt%)	PHI-NSs (10 wt%)
C_1	21.2	16.1	6.61	21.4	19.5	11.7
C_2	23.4	16.2	9.53	23.6	19.7	16.9
$C_2^=$	37.4	25.1	14.4	37.8	30.4	25.5
C_3	6.42	3.47	4.70	6.48	4.19	8.31
$C_3^=$	10.0	5.16	8.16	10.1	6.24	14.4
i-C_4	0	0.407	0	0	0.491	0
n-C_4	0.174	1.36	1.14	0.176	1.64	2.03
$C_4^=$	0.453	14.8	11.9	0.457	17.9	21.1
C_5	0.316	12.4	25.7			
Others	0.601	4.88	17.8			
Sum	100	100	100	100	100	100

Table S7. XRD peak positions and full widths at half maximum for SOD-NSs and conventional SOD crystals.

Peak (2θ)	Full width at half maximum (°)	
	SOD-NSs	Conventional SOD crystals
14.1	0.239	0.218
24.3	0.266	0.321
32.8	0.355	0.391
34.5	0.391	0.412
42.7	0.386	0.482

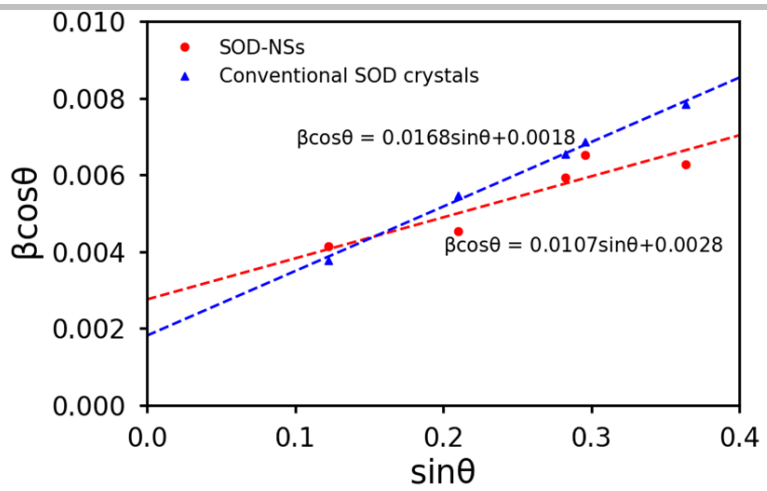

Figure S21. Williamson-Hall plots of SOD-NSs (red) and conventional SOD crystals (blue). In the equations, β is full width at half maximum, η is internal strain, *K* is Scherrer constant, λ is the X-ray wavelength, and *D* is crystallite size. The Scherrer constant used was 0.94. The estimated *D*s for SOD-NSs and conventional SOD crystals are 52 nm and 76 nm, respectively.

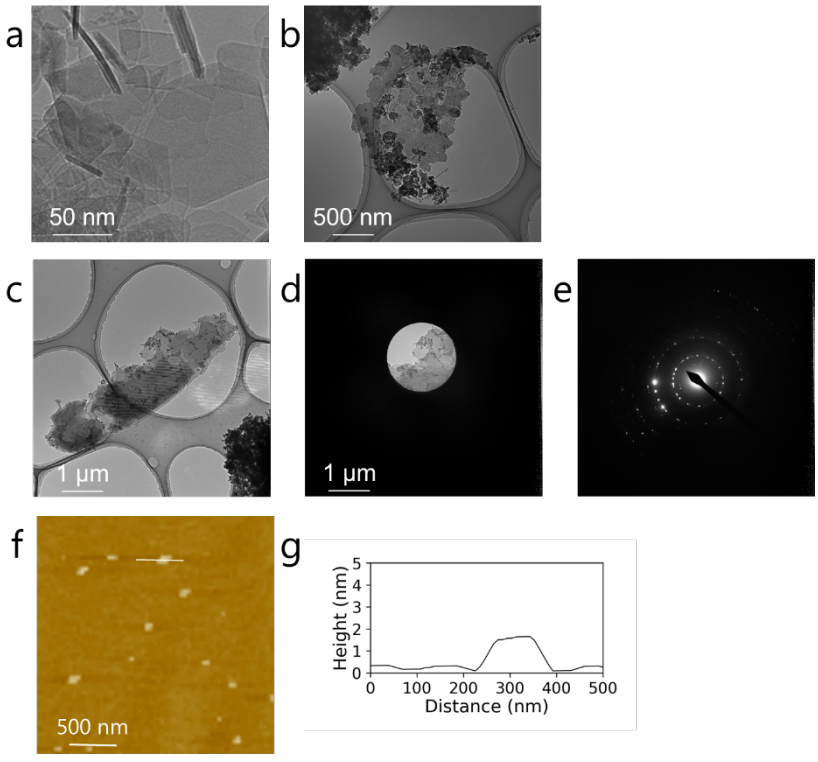

Figure S22. TEM and AFM photographs of SOD-NSs. TEM photographs of a) small SOD-NSs and b) large SOD-NSs. TEM photographs c) without and d) with selected area diffraction aperture. e) SAED patterns. f) AFM photograph and g) cross section of one of the synthesized SOD-NSs.

a

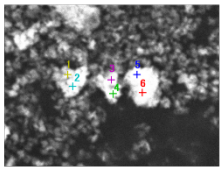

	Na	Al	Si
1	1.29	4.38	4.90
2	1.62	5.33	5.86
3	1.04	3.78	3.80
4	1.37	5.39	5.27
5	1.42	6.13	6.51
6	1.54	6.44	6.81
Average	1.38	5.24	5.53

Si/Al = 1.05

b

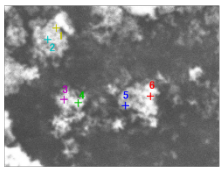

	Na	Al	Si
1	0.15	1.90	3.30
2	0.14	2.17	3.81
3	0.09	1.94	3.44
4	0.10	2.37	4.14
5	0	1.49	2.89
6	0	1.68	3.35
Average	0.12	1.92	3.49

Si/Al = 1.82

Figure S23. SEM-EDX spectra and Si/Al ratio for SOD zeolites. a) conventional SOD particles. b) SOD-NSs.

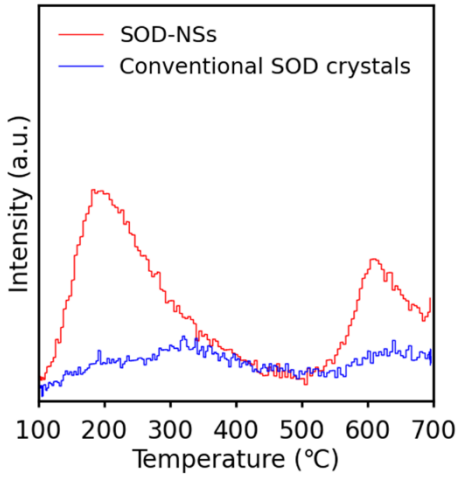

Figure S24. NH_3-TPD profiles of SOD-NSs (red) and conventional SOD crystals (blue).

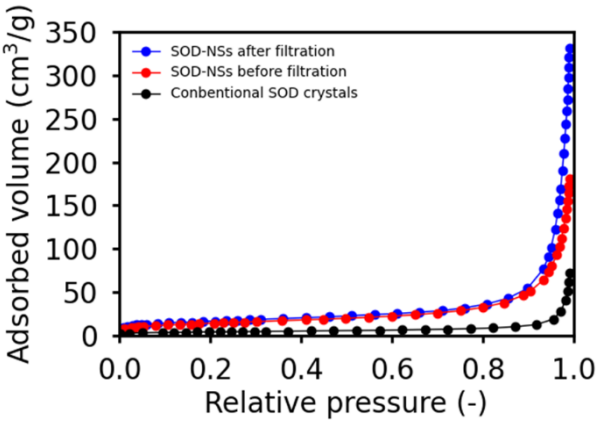

Figure S25. Nitrogen adsorption isotherms for SOD-NSs before (red) and after (blue) filtration and conventional SOD crystals (black).

Table S8. Specific surface area (S_{total}), external surface area (S_{ext}) and pore volume (V_{total}) of conventional SOD crystals, SOD-NSs before filtration, and SOD-NSs after filtration measured by nitrogen adsorption isotherms.

	S_{total}[a] / m^2g^{-1}	S_{ext}[b] / m^2g^{-1}	V_{total}[b] / cm^3g^{-1}
Conventional SOD crystals	15	14	0
SOD-NSs before filtration	50	48	0
SOD-NSs after filtration	59	54	0

[a] Surface area calculated using BET method (BET surface area) applied to the nitrogen adsorption isotherm.

[b] S_{ext} and V_{total} calculated using the *t*-plot method applied to the nitrogen adsorption isotherm.

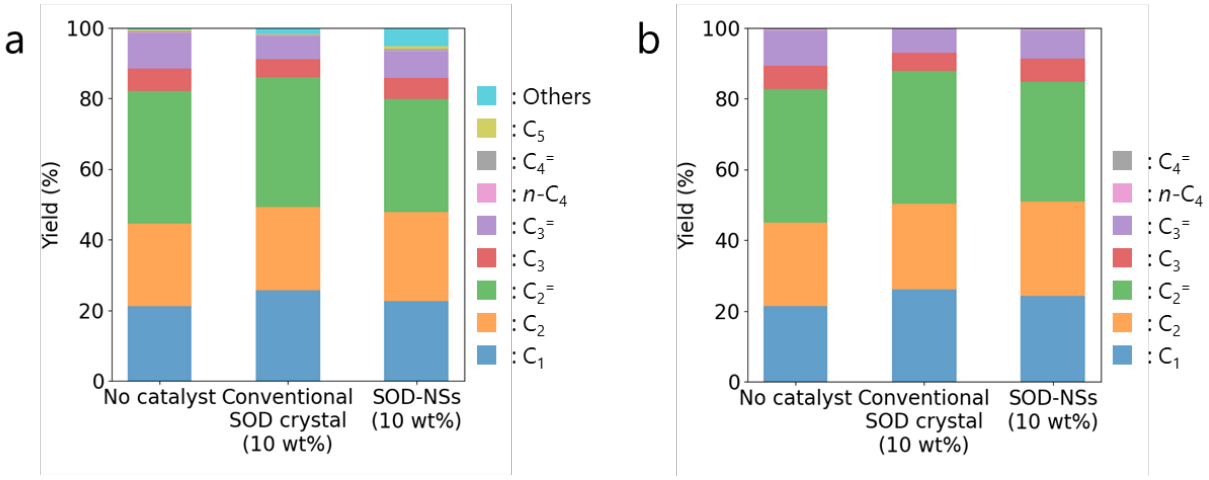

Figure S26. Product distribution in LDPE cracking reactions without and with conventional SOD crystals (10 wt%) or SOD-NSs (10 wt%). Product distribution a) with and b) without large molecules.

Table S9. Product distribution in LDPE cracking reaction without any catalysts and with conventional SOD crystals (10 wt%) or SOD-NSs (10 wt%). Product distribution with (left side) and without (right side) large molecules.

	No catalyst	Conventional SOD crystals (10 wt%)	SOD-NSs (10 wt%)	No catalyst	Conventional SOD crystals (10 wt%)	SOD-NSs (10 wt%)
C_1	21.2	25.6	22.7	21.4	26.1	24.1
C_2	23.4	23.6	25.2	23.6	24.1	26.8
$C_2^=$	37.4	36.7	31.9	37.8	37.5	33.9
C_3	6.42	5.07	6.06	6.48	5.17	6.44
$C_3^=$	10.0	6.65	7.61	10.1	6.79	8.09
i-C_4	0	0	0	0	0	0
n-C_4	0.174	0.154	0.107	0.176	0.157	0.114
$C_4^=$	0.453	0.151	0.514	0.457	0.154	0.546
C_5	0.316	0.335	0.693			
Others	0.601	1.69	5.27			
Sum	100	100	100	100	100	100

Table S10. XRD peak positions and full widths at half maximum for MFI-NSs and conventional MFI crystals.

Peak (2θ)	Full width at half maximum (°)	
	MFI-NSs	Conventional MFI crystals
8.0	0.130	0.123
8.9	0.171	0.147
13.9	0.169	0.112
14.8	0.169	0.135
17.8	0.160	0.120
20.8	0.162	0.171
23.1	0.204	0.109
23.4	0.130	0.189

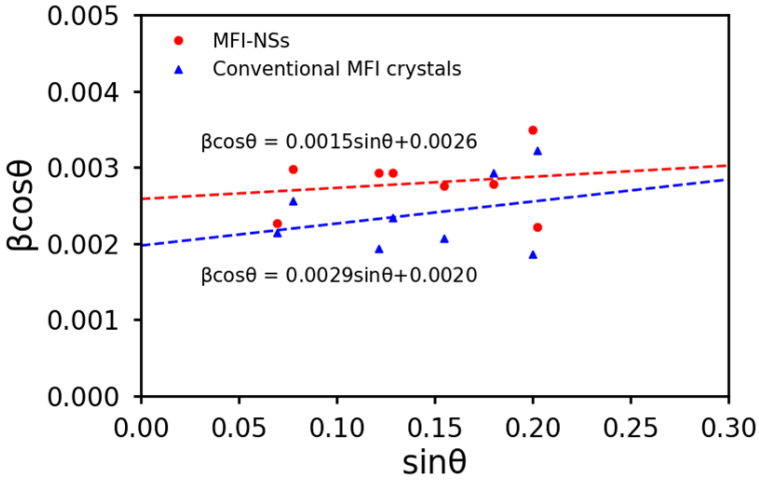

Figure S27. Williamson-Hall plots of MFI-NSs (red) and conventional MFI crystals (blue). In the equations, β is full width at half maximum, η is internal strain, *K* is Scherrer constant, λ is the X-ray wavelength, and *D* is crystallite size. The Scherrer constant used was 0.94. The estimated *D*s for MFI-NSs and conventional MFI crystals are 56 nm and 72 nm, respectively.

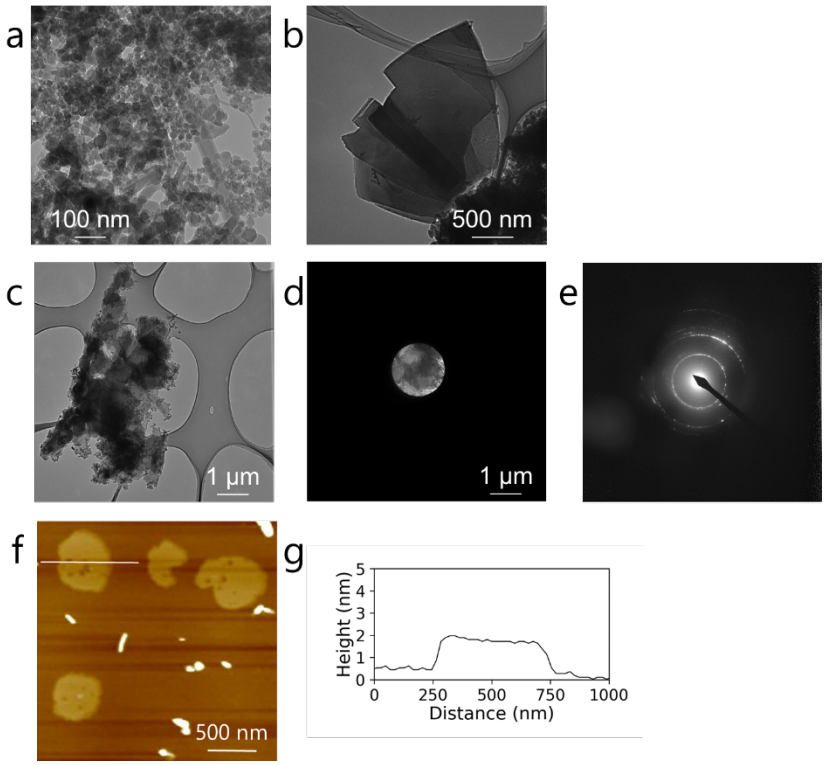

Figure S28. TEM and AFM photographs of MFI-NSs. TEM photographs of a) small MFI-NSs and b) large MFI-NSs. TEM photographs c) without and d) with selected area diffraction aperture. e) SAED pattern. f) AFM photograph and g) cross section of one of the synthesized MFI-NSs.

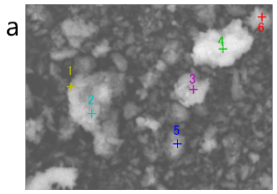

	Al	Si
1	1.71	17.15
2	1.65	16.50
3	1.58	15.69
4	1.49	15.07
5	1.77	17.88
6	2.15	23.08
Average	1.72	17.56

Si/Al = 10.2

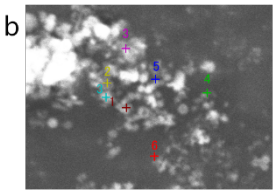

	Al	Si
1	13.62	86.38
2	19.71	80.29
3	11.15	88.85
4	12.60	87.40
5	15.25	84.75
6	16.32	83.68
7	12.42	87.58
Average	14.44	85.56

Si/Al = 5.9

Figure S29. SEM-EDX spectra and Si/Al ratio for MFI zeolites. a) Conventional MFI particles. b) MFI-NSs..

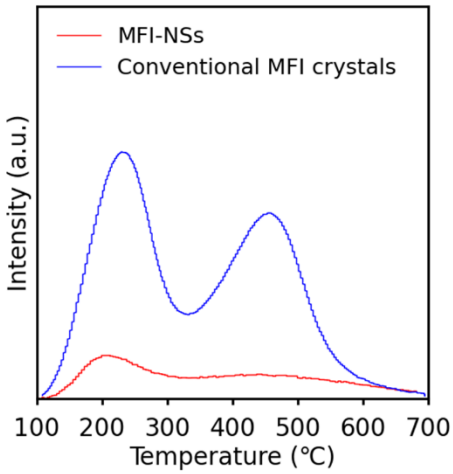

Figure S30. NH_3-TPD profiles of MFI-NSs (red) and conventional MFI crystals (blue).

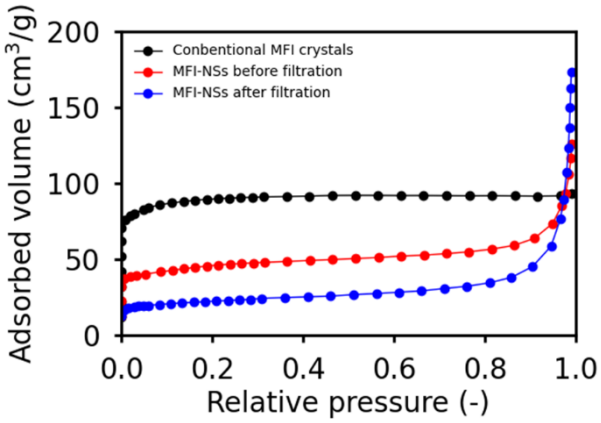

Figure S31. Nitrogen adsorption isotherms for MFI-NSs before (red) and after (blue) filtration and conventional MFI crystals.

Table S11. Specific surface area (S_{total}), external surface area (S_{ext}) and pore volume (V_{total}) of conventional MFI crystals, MFI-NSs before filtration and MFI-NSs after filtration measured by nitrogen adsorption isotherms.

	S_{total}[a] / m^2g^{-1}	S_{ext}[b] / m^2g^{-1}	V_{total}[b] / cm^3g^{-1}
Conventional MFI crystals	405	0.09	0.14
MFI-NSs before filtration	165	24	0.06
MFI-NSs after filtration	81	37	0.02

[a] Surface area calculated using BET method (BET surface area) applied to the nitrogen adsorption isotherm.

[b] S_{ext} and V_{total} calculated using the *t*-plot method applied to the nitrogen adsorption isotherm.

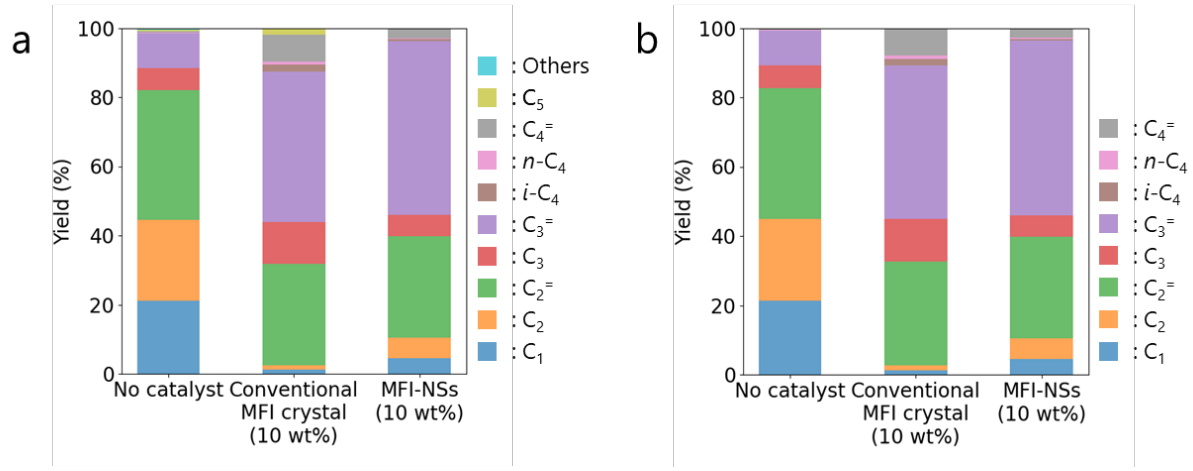

Figure S32. Product distribution in LDPE cracking reaction without and with conventional MFI crystals (10 wt%) or MFI-NSs (10 wt%). Product distribution a) with and b) without large molecules.

Table S12. Product distribution in LDPE cracking reaction without any catalysts and with conventional MFI crystals (10 wt%) or MFI-NSs (10 wt%). Product distribution with (left side) and without (right side) large molecules.

	No catalyst	Conventional MFI crystals (10 wt%)	MFI-NSs (10 wt%)	No catalyst	Conventional MFI crystals (10 wt%)	MFI-NSs (10 wt%)
C_1	21.2	1.16	4.60	21.4	4.60	1.19
C_2	23.4	1.38	5.83	23.6	5.83	1.40
$C_2^=$	37.4	29.3	29.3	37.8	23.0	29.3
C_3	6.42	12.0	6.28	6.48	12.3	6.28
$C_3^=$	10.0	43.5	50.3	10.1	44.2	50.3
i-C_4	0	1.97	0.598	0	2.02	0.576
n-C_4	0.174	0.853	0.265	0.176	0.873	0.261
$C_4^=$	0.453	7.80	2.69	0.457	7.95	2.85
C_5	0.316	1.76	0.007			
Others	0.601	0.238	0.190			
Sum	100	100	100	100	100	100

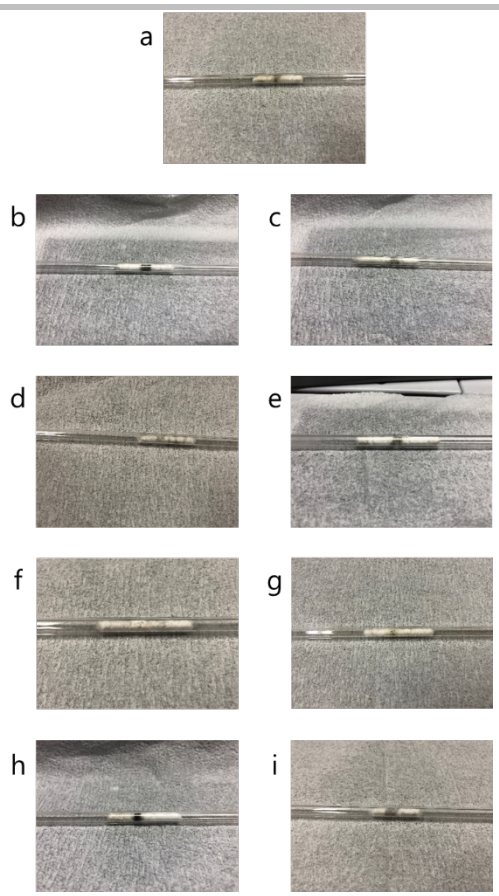

Figure S33. Quartz glass capillaries with the samples after the catalytic test: a) No catalyst. b) Conventional CHA crystals (10 wt%). c) CHA-NSs (10 wt%). d) Conventional PHI crystals (10 wt%). e) PHI-NSs (10 wt%). f) Conventional SOD crystals (10 wt%). g) SOD-NSs (10 wt%). h) Conventional MFI crystals (10 wt%). i) MFI-NSs (10 wt%).